On the Structure of the Southern Oscillation

YI CHAO* AND S. G. H. PHILANDER

Atmospheric and Oceanic Sciences Program, Princeton University, Princeton, New Jersey

(Manuscript received 9 September 1991, in final form 29 May 1992)

ABSTRACT

A realistic oceanic general circulation model is forced with winds observed over the tropical Pacific between 1967 and 1979. The structure of the simulated Southern Oscillation is strikingly different in the western and eastern sides of the basin, because the principal interannual zonal-wind fluctuations are confined to the west and are in the form of an equatorial jet. This causes thermocline displacements to have maxima off the equator in the west (where the curl of the wind is large) but on the equator in the east. Zonal phase propagation, both on and off the equator, is at different speeds in the west and east. The phase pattern is complex, and there is, on interannual time scale, no explicit evidence of individual equatorial waves. These results lead to a modification of the "delayed oscillator" mechanism originally proposed by Schopf and Suarez to explain a continual Southern Oscillation. The results also permit an evaluation of the various coupled ocean–atmosphere models that simulate the Southern Oscillation and indicate which measurements are necessary to determine which models are most relevant to reality.

1. Introduction

Bjerknes (1969) first proposed that the Southern Oscillation is attributable to interactions between the ocean and atmosphere. Numerous subsequent studies have put this hypothesis on a firm footing [see Philander (1990) for a review]. Particularly important are the data analysis of Wyrtki (1975), who established how changes in the surface winds affect sea level, and the analysis of Rasmusson and Carpenter (1982), who described the tropical atmospheric response to the changing sea surface temperatures. The studies just mentioned focus on the evolution of the warm El Niño phase of the Southern Oscillation and thus promote the idea that El Niño is an isolated, sporadic occurrence. It is viewed as a departure from otherwise normal conditions that develops in response to "triggers" such as westerly wind bursts over the western equatorial Pacific. Figure 1 illustrates possible responses to an initial burst of westerly winds that persists over the western equatorial Pacific for a month. These are simulations with the coupled model of Neelin (1990). In Fig. 1a the coupled system is weakly unstable, and air–sea interactions lead to the development of El Niño, which later decays. Nothing further happens until a new perturbation initiates new developments. The situation is very different in Fig. 1b, where the system is sufficiently unstable to support self-sustaining oscillations, and in Fig. 1c, where it is so unstable that secondary instabilities appear. The parameters that can affect a transition from the conditions in Fig. 1a to 1b to 1c are numerous and include the mean depth of the thermocline and the mean zonal sea surface temperature gradient. If El Niño is viewed as a sporadic departure from otherwise "normal" conditions, then the appropriate parameter range for the Pacific corresponds to that of Fig. 1a.

Available time series measurements (of sea level pressure at Darwin and Easter islands, for example) suggest that El Niño should be regarded, not as an isolated, sporadic occurrence, but as one phase of a continual, irregular cycle, the Southern Oscillation. Bjerknes (1969) subscribed to this view, which implies that the appropriate parameter range for the Pacific is not that of Fig. 1a but that of Fig. 1b. It then becomes necessary to identify the processes that keep the oscillation going and that determine its period. Schopf and Suarez (1988) were the first to do this for the interannual oscillations that occur in their coupled ocean–atmosphere model. The proposed mechanism involves oceanic waves, but efforts to observe these phenomena appear to be handicapped by the paucity of subsurface oceanic data. Several investigators have tried to finesse this difficulty by exploiting the realism with which numerical models simulate the tropical oceans when forced with observed winds. Pares-Sierra et al. (1985), Pazan et al. (1986), White and Pazan (1987), Zebiak (1989), and Wakata and Sarachik (1991) use shallow-water models, which are good at reproducing thermocline displacements. Latif and Flügel (1990) and

* *Present affiliation:* The University of California at Los Angeles.

Corresponding author address: Dr. Yi Chao, Department of Atmospheric Sciences, University of California, Los Angeles, 405 Hilgard Avenue, Los Angeles, CA 90024-1565.

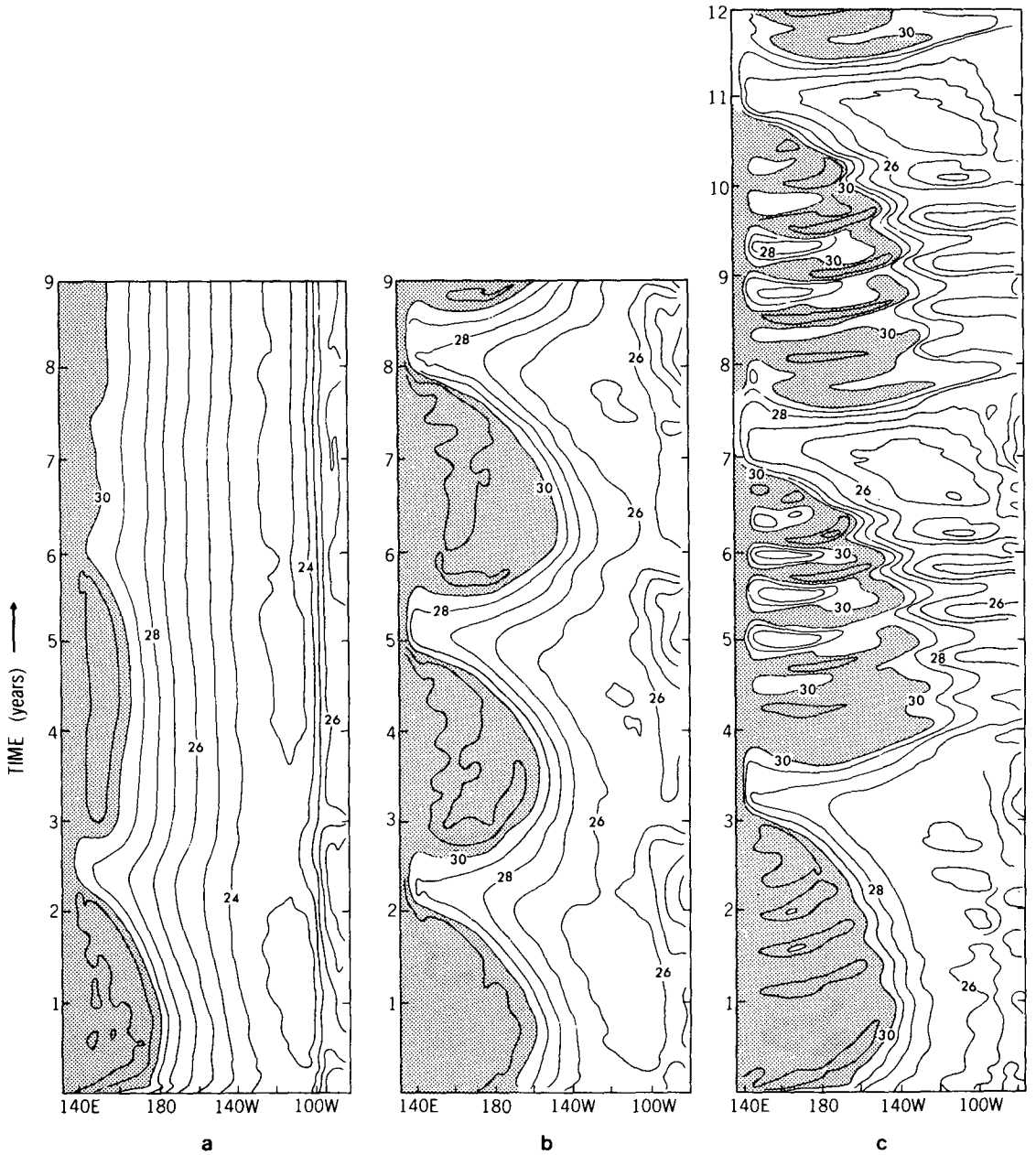

FIG. 1. Isotherms (°C) along the equator over a period of years in the coupled ocean–atmosphere model of Neelin (1990). Westerly winds are imposed over the western side of the basin for a month, whereafter ocean–atmosphere interactions, which are weak (a), moderately strong (b), and very strong (c), control further developments. The strength of the interactions is increased by increasing the drag coefficient that converts wind speed to stress.

Kitamura (1990) use general circulation models (GCM), which, in addition to thermocline displacements, simulate oceanic currents and thermal fields realistically. These various studies presumably all yield similar results, but each investigation involves different methods of analysis and focuses on different aspects of the phenomenon so that the approach in which a realistic model is forced with observed winds is not exhausted yet. There are, furthermore, inconsistencies that need to be resolved. If the appropriate parameter range for the Pacific is that of Fig. 1a, then the critical "triggers," such as westerly wind bursts, excite oceanic waves such as equatorial Kelvin waves that are readily identifiable. If, however, the relevant parameter range is that of Fig. 1b, and if the period of the continual oscillation is on the order of 3 years, then the winds excite a host of oceanic waves that are superimposed. The resultant phase field will then be so complex that

individual oceanic waves cannot be identified. Yet Schopf and Suarez (1988) and other investigators seem to identify explicitly the equatorial Kelvin and Rossby waves that keep the oscillation going. Is something amiss? This paper examines the matter and explores aspects of the Southern Oscillation that were overlooked by earlier investigators.

One of our goals is to comment on the various coupled ocean–atmosphere models that simulate Southern Oscillations: those of Zebiak and Cane (1987), Battisti (1988), Schopf and Suarez (1988), Meehl (1990), Lau et al. (1992), and Philander et al. (1992). Each of these simulations has realistic features, but they nonetheless are significantly different from each other. Which, if any, are the most relevant to reality? The results from a realistic oceanic model can shed light on this matter, not by answering the question directly but by indicating which measurements are necessary to answer this question.

Section 2 of this paper describes the model and forcing functions that are used. Sections 3 and 4 describe the structure of the Southern Oscillation. The heat budget is the topic of section 5. Conclusions and comments on different models are presented in section 6.

2. The model

This study uses the oceanic GCM developed by Bryan (1969) and Cox (1984) and later modified for the tropical Pacific as in the study by Philander et al. (1987). The parameterization of vertical mixing is the one proposed by Pacanowski and Philander (1981). The coefficients of horizontal eddy viscosity and diffusivity have the constant value 10^7 cm^2 s^{-1}. The model, for the tropical Pacific, extends from 45°S to 55°N and has the idealized eastern and western coasts shown in Fig. 2. The resolution is 1.5° longitude and 1/3° latitude between 10°S and 10°N, but 1° latitude farther poleward. There are 27 levels in the vertical, with 9 of those in the upper 300 m. The first few are 10 m deep. Topography is taken into account, but the ocean is nowhere deeper than 4000 m, and islands are sunk so that their tops are 65 m below sea level.

The initial conditions correspond to the climatological temperature and salinity data described by Levitus (1982), and there are no currents. Near the artificial northern and southern boundaries these climatological conditions are maintained throughout the integrations. In the regions poleward of 35°S and 45°N, the equations for temperature and salinity acquire additional terms to damp these fields toward climatological values. The currents vanish at the northern and southern boundaries. No flux of heat and salt is allowed on the east and west boundaries. A no-slip condition is applied at lateral walls.

There is zero heat flux through, and no motion at the ocean floor. At the ocean surface the wind stress and heat flux, parameterized in terms of wind speed and air–sea temperature difference as in Philander et al. (1987), are specified. During the first three years, by which time quasi-equilibrium conditions are attained, the forcing corresponds to the COADS climatology. Thereafter, monthly mean COADS data for the period 1967–1979, as described by Oort et al. (1987), force the model.

The simulation, when compared with the few available measurements, is reasonably realistic. In Fig. 2, which shows the climatological sea surface temperature patterns at the extremes of the seasonal cycle, it is evident that simulated temperatures along the equator are too low, especially during periods of light winds in March. Off the equator simulated temperatures are too high, but generally are within 1°C of the observed values. The simulation of interannual sea surface temperature fluctuations along the equator, shown in Fig. 3, are remarkably accurate, and the model realistically reproduces the succession of El Niño and La Niña episodes. Heat storage variations, as shown in Fig. 4 at the location of the Galapagos Islands, are in good agreement with the observed sea level, which is a good surrogate of the heat storage (Rebert et al. 1985; Chao 1990). Seasonal fluctuations of the surface currents and Equatorial Undercurrent are also realistic and are described elsewhere (Chao 1990; Philander and Chao 1991).

The annual mean surface wind stress, sea surface temperature, and heat storage are shown in Fig. 5. The zonal-wind component is westward over most parts of the Pacific basin. The meridional wind component is northward south of 8°N and equatorward north of 8°N. In response to the surface winds, broad features of the equatorial Pacific are reproduced: high sea surface temperatures are located in the western equatorial Pacific and low sea surface temperatures in the eastern Pacific; there is a cold tongue along the equator extending from the coast of Central America to the central Pacific with the lowest temperature of 24°C; warm waters near 8°N extend from the eastern Pacific to the western equatorial Pacific. The characteristic features of the heat storage distribution are also realistically simulated compared with the XBT data (White et al. 1985; Kessler 1990): regions of maximum heat storage are located in the western Pacific near 20°N and 10°S; along the equator heat storage increases in a westward direction; a minimum in the heat storage near 10°N extends across the Pacific basin. The climatological seasonal cycle is described elsewhere (Chao 1990; Philander and Chao 1991).

The rest of this paper describes strictly interannual fluctuations. Plots of anomalous conditions at a certain time, of time dependence, or of analyzed fields, such as empirical orthogonal functions, were obtained from the model's original time series by removing the mean and then low-pass filtering to remove fluctuations with

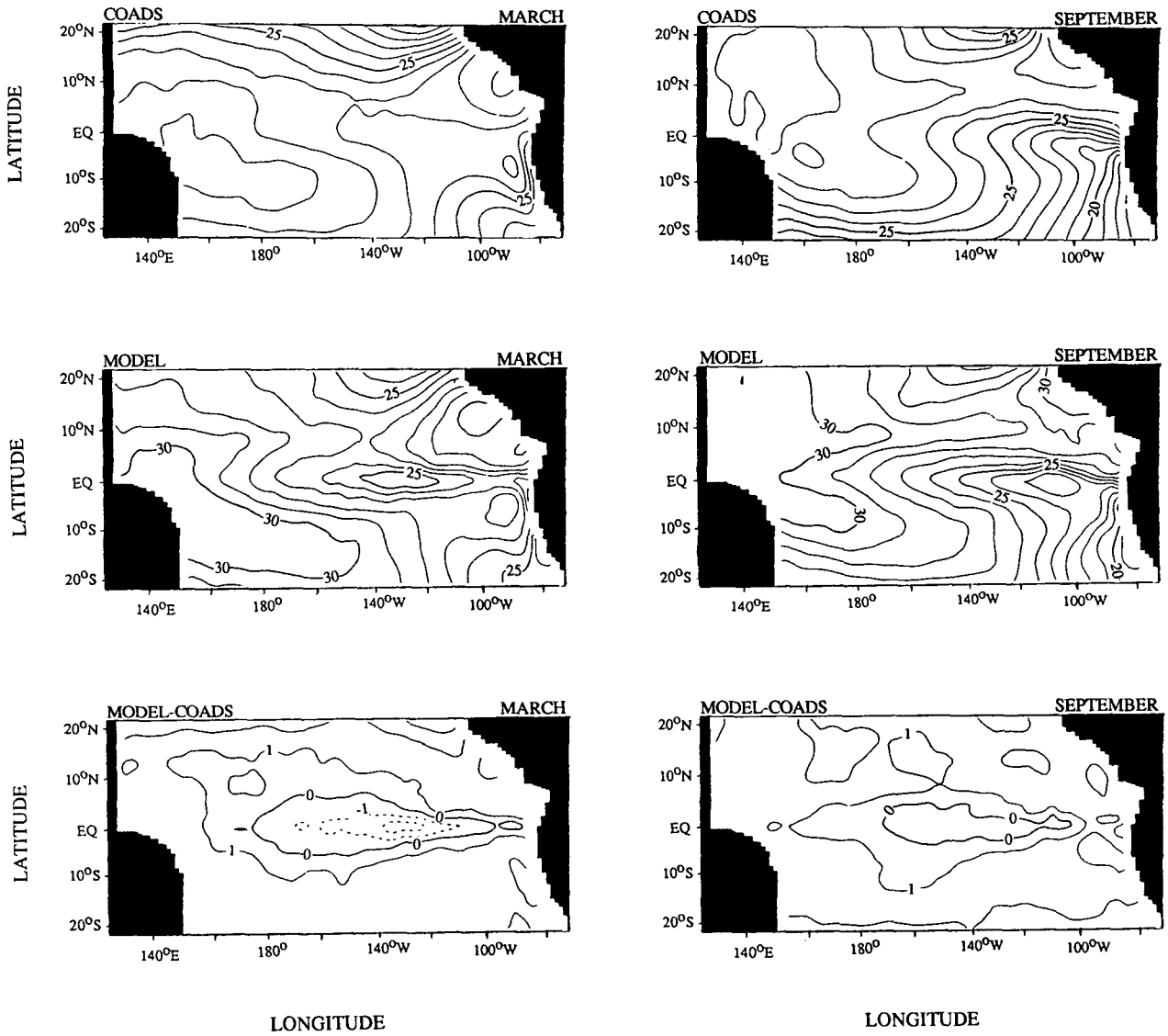

FIG. 2. Monthly mean maps of sea surface temperature (°C) in March and September from the observation of COADS, the model simulation and the model minus observation. Solid lines indicate warm waters, and dashed lines indicate cold waters.

a period less than 2 years. For more details the reader is referred to Chao (1990).

3. Interannual variations

In Fig. 3 it is clear that the most intense El Niño during the period under consideration occurred in 1972 and was preceded and followed by intense, cold La Niña episodes. We therefore start by focusing on the period from January 1971 when La Niña conditions prevailed, to June 1973, by which time El Niño had come and gone and La Niña had reappeared. Figures 6, 7, and 8 are sequences of maps of the surface wind, sea surface temperature, and heat storage anomalies, at six monthly intervals, between January 1971 and June 1973. The maps for January 1971 and July 1972 contrast La Niña and El Niño. A striking feature of the surface wind field (in Fig. 6) on these two occasions is the narrow equatorial jet to the west of approximately 140°W. It is westerly during the warm episode, easterly during the cold one. Harrison's (1987) analysis of wind records from islands in the western tropical Pacific Ocean confirmed the jet structure. Given this distinctive feature of the wind fluctuations, it can be expected that the oceanic response to these winds will also be distinctive. The latitudinal shear of the jets in the west implies Ekman pumping that should cause large vertical excursions of the thermocline toward 10°N and S in the west. Figures 8 and 9 confirm this inference when the atmospheric jets are present. The off-equa-

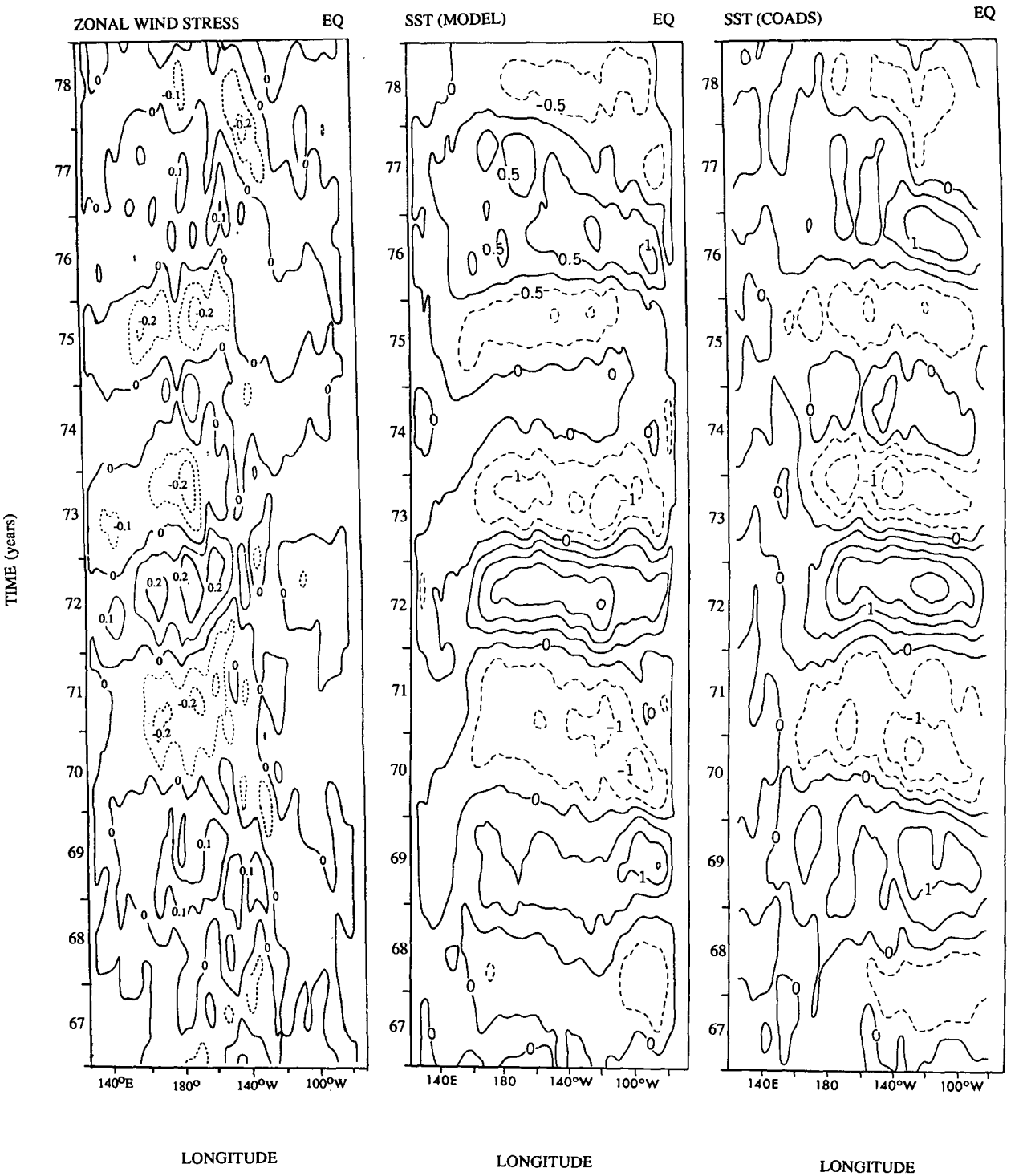

FIG. 3. Interannual zonal wind stress (dyn cm^{-2}) and sea surface temperature (°C) anomalies along the equator between 1967 and 1978.

torial maxima of the thermocline displacements in the west are in sharp contrast to the equatorially centered thermocline displacements in the east. The reason for the change from west to east is the absence of significant interannual wind variations in the east. The winds in the west influence conditions in the east by means of equatorial Kelvin waves that are centered on and that are symmetrical about the equator—hence the ap-

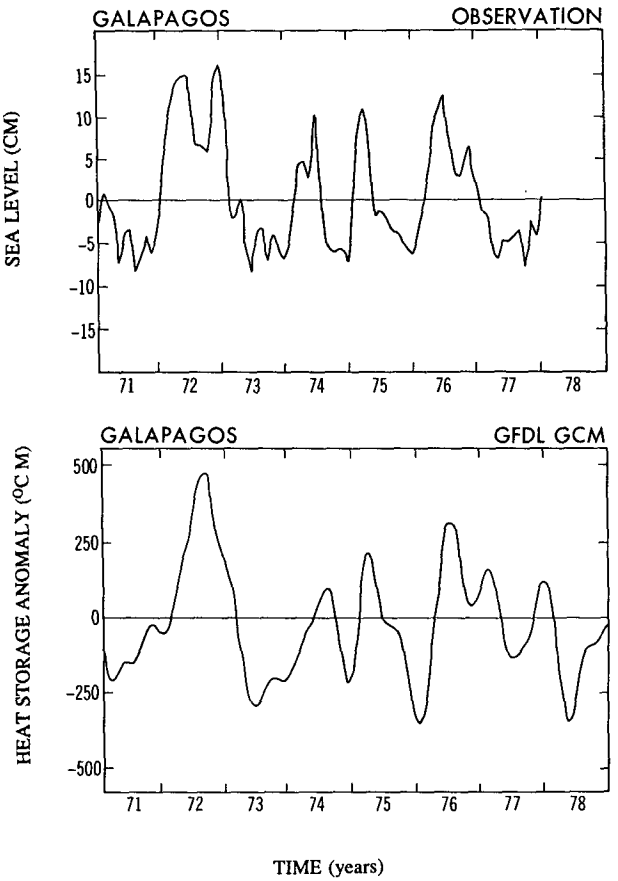

FIG. 4. Time series of sea level anomalies at Galapagos (0.5°S, 90.3°W) between 1971 and 1978 from the observation of Wyrtki (1975) and the model simulated heat storage that corresponds to the vertically integrated temperature in the upper 300 m.

proximate Gaussian shapes of thermocline displacements in the east in Figs. 8 and 9. The apparent northward phase propagation of heat storage anomalies (Fig. 9) can be attributed to the latitudinal variation of the Coriolis parameter (Schopf et al. 1981).

The winds have a distinctive structure at the peaks of El Niño and La Niña, but during the transition periods, January 1972 and June 1973, for example, neither the surface winds (Fig. 6) nor the sea surface temperature anomalies (Fig. 7) seem particularly organized, although in thermocline displacements (Fig. 8) there is a tendency for distinctive zonal bands to appear.

Changes in the depth of the thermocline affect sea surface temperature only in regions where the thermocline is relatively shallow. Along the equator this is the case in the eastern half of the Pacific, as is evident in Fig. 5, so that the largest sea surface temperature fluctuations (in Fig. 7) occur in that region where local wind variations are slight. Figure 3 confirms that interannual variations in sea surface temperature tend to appear in the central and eastern equatorial Pacific while the zonal-wind variations are predominantly in the west.

During the Southern Oscillation there is a significant zonal transfer of warm surface waters across the tropical Pacific. A plot of variations of the surface currents across 170°E and 130°W, in Fig. 10, indicates anomalous eastward surface currents during El Niño and westward surface currents during La Niña. The changes have a larger amplitude in the west (where the large zonal-wind variations occur) than east. Figures 11 and 12 depict the vertical structure of these changes. Near the equator in the west the currents are to a large extent attributable to the zonal component of the wind and its curl. However, anomalies of the meridional component of the wind are also important. They are southerly during La Niña (July 1971 in Fig. 6) and northerly during El Niño (July 1972 and January 1973 in Fig. 6), and correspond to a northward (during La Niña) or southward (during El Niño) displacement of the intertropical convergence zone (ITCZ).

Between La Niña and El Niño the Equatorial Undercurrent weakens more in the west (Fig. 11) than in the east (Fig. 12). The section along the equator in Fig. 13 explains why. The changes in the zonal wind in the west cause the zonal slope of the thermocline (with which is associated the pressure force that drives the Equatorial Undercurrent) to change significantly in that region, but the slope does not vary as much in the east, although the depth of the thermocline increases from La Niña to El Niño. This result is also evident in Fig. 14, which illustrates that zonal phase propagation is very nonuniform in longitude, both on and off the equator.

Heat-storage anomalies along the equator, shown in the central panel of Fig. 14, have an eastward phase propagation at a speed of approximately 20 cm s^{-1}, but only in the western half of the basin. In the east, along the equator, changes are practically instantaneous. Off the equator phase propagation is westward and is relatively slow in the east but is much more rapid to the west of the date line. Nowhere does the phase speed correspond to that of individual low-order baroclinic waves. The phase speed along the equator in the west is an order of magnitude slower than that of the expected Kelvin wave. Near 9°N and S in the east the westward speed of approximately 7 cm s^{-1} is slower than that of the expected Rossby waves. The reason for the absence of explicit evidence of individual, free oceanic waves can be found in numerous studies of the oceanic response to periodic forcing. At low frequencies the response is composed of directly forced motion plus a host of waves, each of which has a distinctive phase speed. In the case of special forcing functions, this superposition can lead to intriguing phenomena such as foci (Cane and Sarachik 1981; Schopf et al. 1981) and beams (McCreary 1984). In general, the superposition leads to complex phase fields

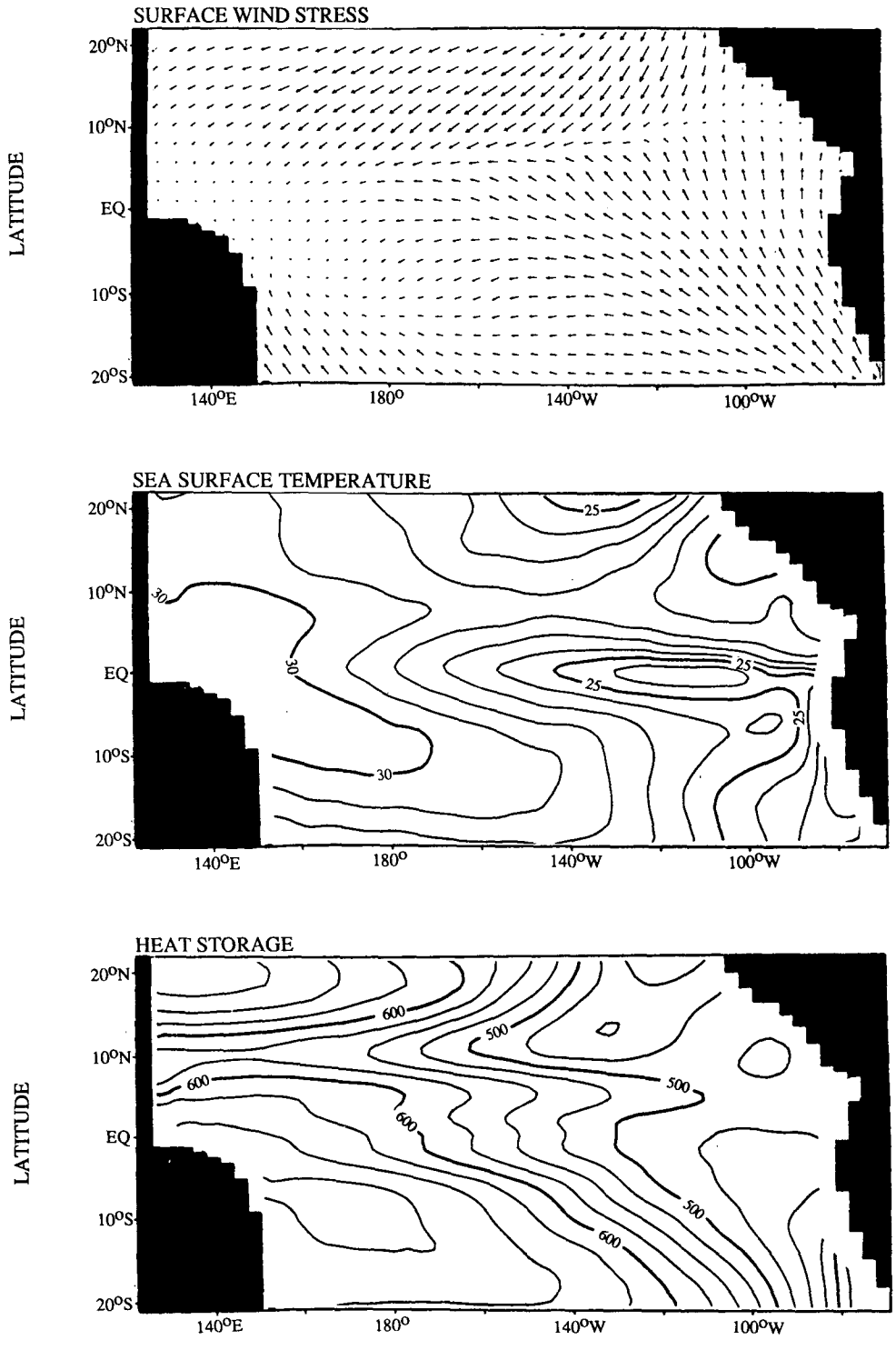

FIG. 5. The annual mean surface wind stress (from COADS), model simulated sea surface temperature (°C), and heat storage (represented by vertically averaged temperature in the upper 300 m and in unit of 10^1 °C m).

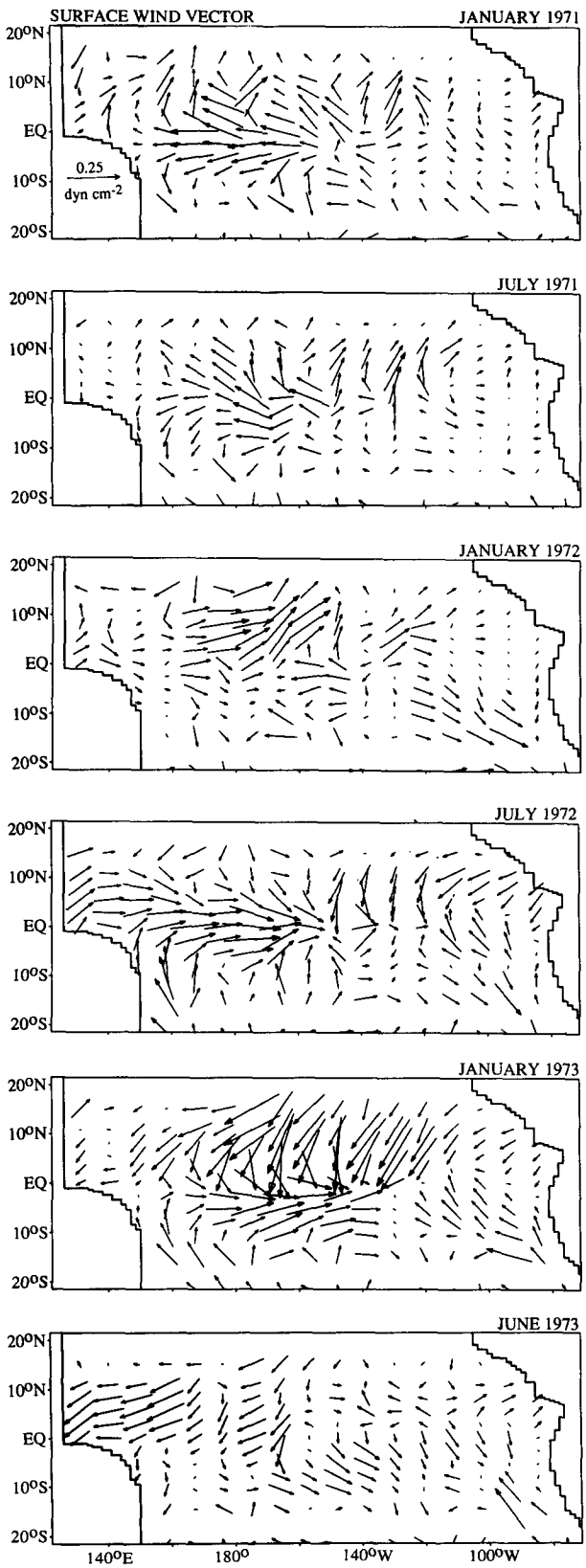

FIG. 6. Six monthly maps of surface wind stress from COADS between January 1971 and June 1973. The data have been low-pass filtered to remove fluctuations with a period less than 2 years.

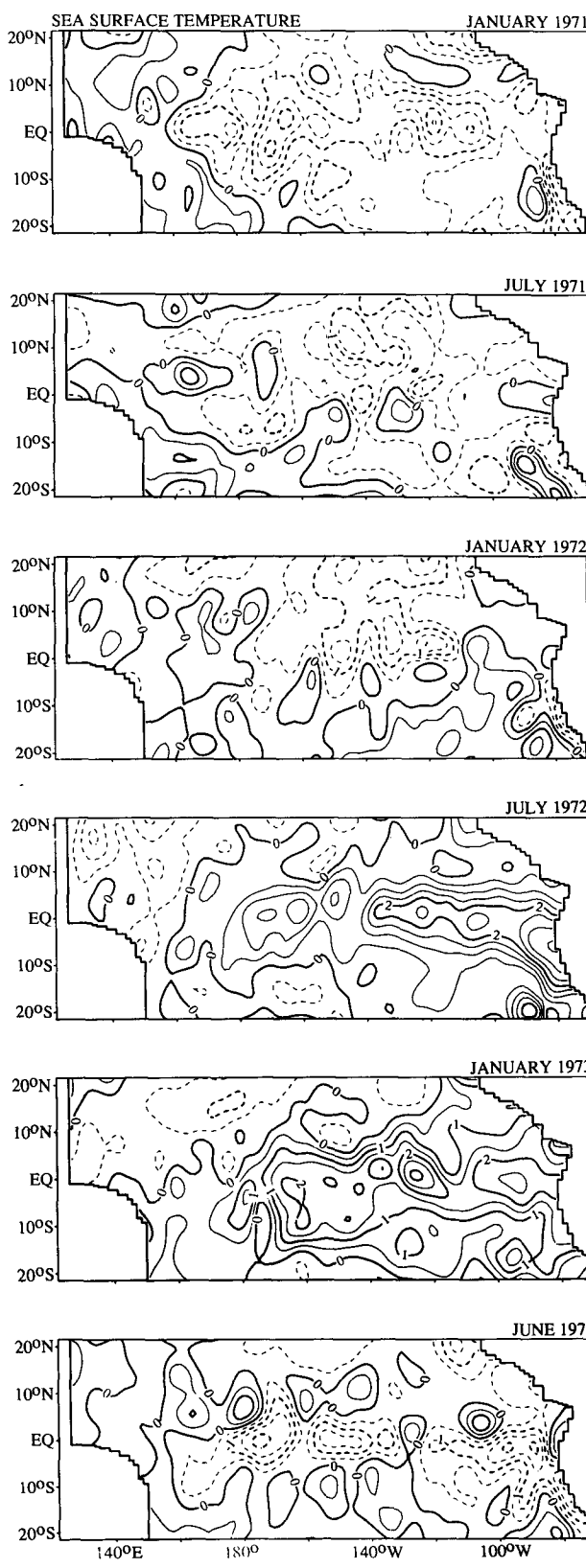

FIG. 7. The same as Fig. 6 but for sea surface temperature (°C). Solid lines indicate warm waters, and dashed lines indicate cold waters.

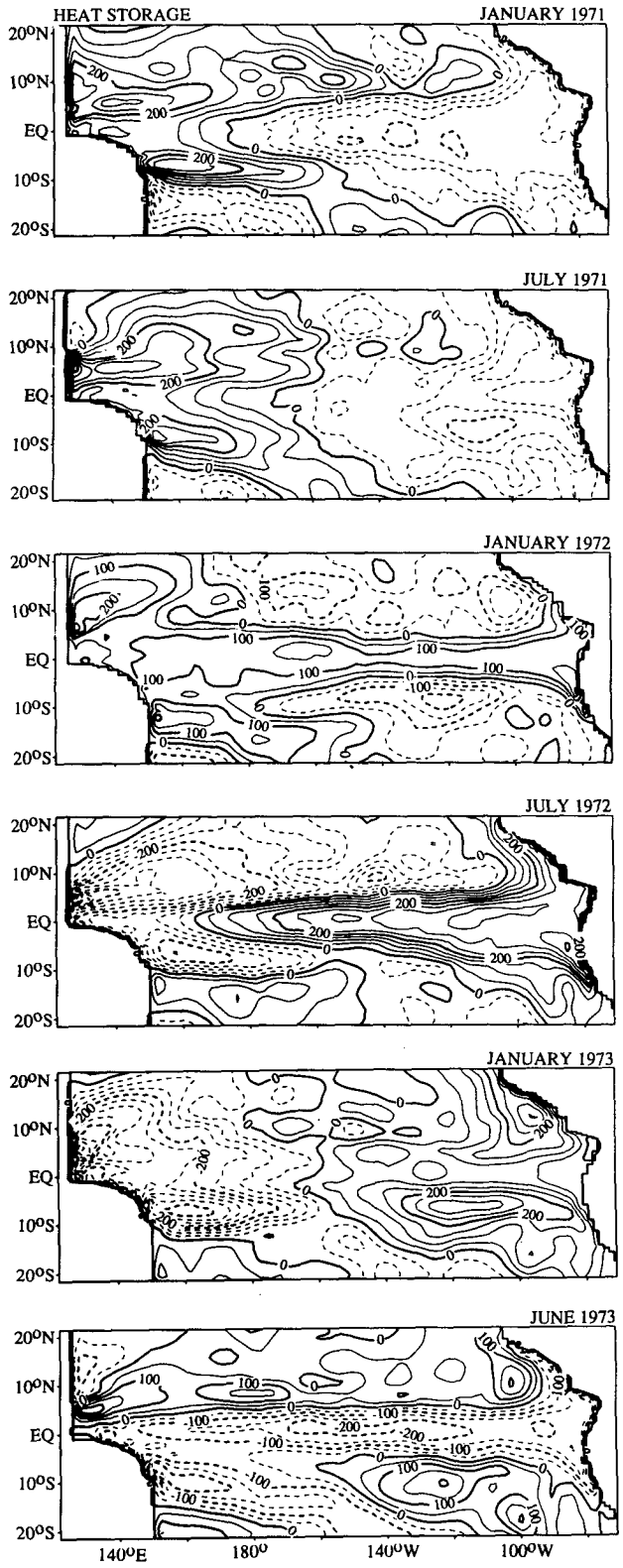

FIG. 8. The same as Fig. 6 but for model simulated heat storage (°C cm). Solid lines indicate deepening of the thermocline, and dashed lines indicate shoaling.

such as those in Fig. 14, where individual waves cannot be identified. The phases in the west differ from those in the east because the motion forced directly by the wind is predominantly in the west where wind fluctuations have their largest amplitude. Off the equator in the west the wind influences both the phase and amplitude. The large vertical fluctuations of the thermocline in that region are not merely Rossby waves that arrived from the east but to a large extent are locally forced disturbances.

The phase of the oceanic response to periodic forcing simplifies as the forcing period increases. It is particularly simple in the extreme case of forcing at a period much longer than the adjustment time of the ocean. In that case the ocean possesses no "memory" and there is no explicit evidence of phase propagation. In other words, at each moment the oceanic response is in equilibrium with the forcing (Philander and Pacanowski 1981). It is clear from Fig. 14 that this is not the case on the time scale of the Southern Oscillation. This nonequilibrium oceanic response associated with the Southern Oscillation is very important because it is the "memory" that the ocean has of earlier winds that causes the termination of one phase of the Southern Oscillation and that introduces the next.

If, in July 1972, the ocean had been in equilibrium with the winds at that time then persistence of those winds would have caused El Niño conditions to persist. It is evident from Fig. 14, however, that in July 1972 the ocean was not in equilibrium with the winds at the time but was still adjusting to earlier changes in the wind. Even if the winds had remained unchanged after July 1972, the equatorial thermocline in the west would have continued shoaling as the off-equatorial elevations of the thermocline (in Fig. 8) dispersed equatorward. Subsequently the elevations would have dispersed to the east causing shallower thermocline, which would presumably decrease sea surface temperatures and in turn affect the atmosphere. Weaker westerly winds in the west would reinforce the shoaling of the thermocline and the lowering of sea surface temperatures in the east. In due course, El Niño would terminate and La Niña would start to develop.

4. Extended empirical orthogonal function analyses

The description of the Southern Oscillation in section 3 is for the period January 1971–June 1973. Inspection of similar figures for other periods indicate that the description is also valid for other times. To confirm this, we performed an empirical orthogonal function (EOF) analysis for the entire time series generated by the model. A conventional EOF analysis gives results consistent with those of section 3, but such an analysis is more appropriate for stationary than for propagating patterns. We therefore adopted the extended EOF technique, which Weare and Nastrom (1982) and Lau and Chan (1985) describe in detail.

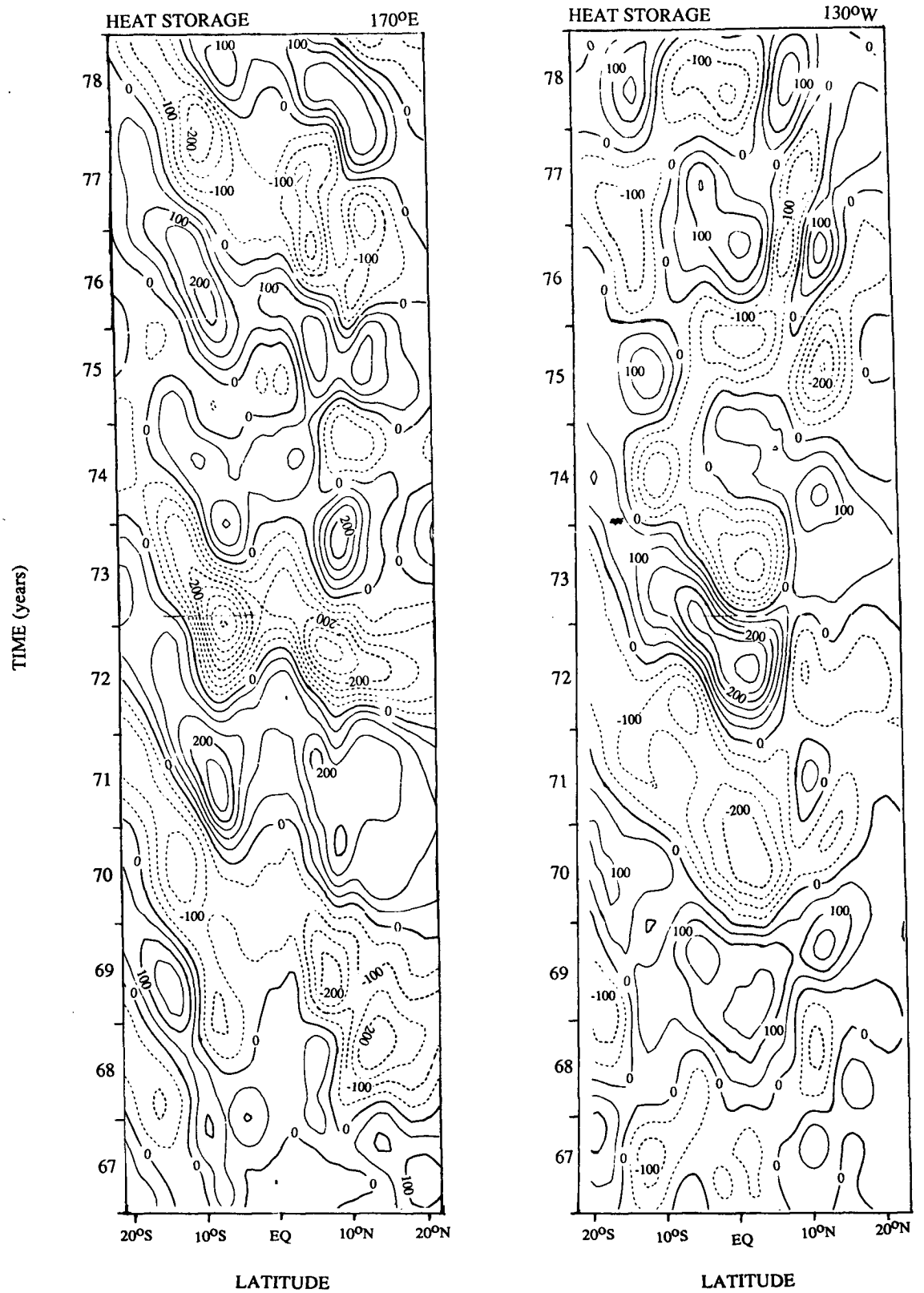

FIG. 9. Interannual variations in heat storage (°C m) at 170°E in the western and 130°W in the eastern tropical Pacific.

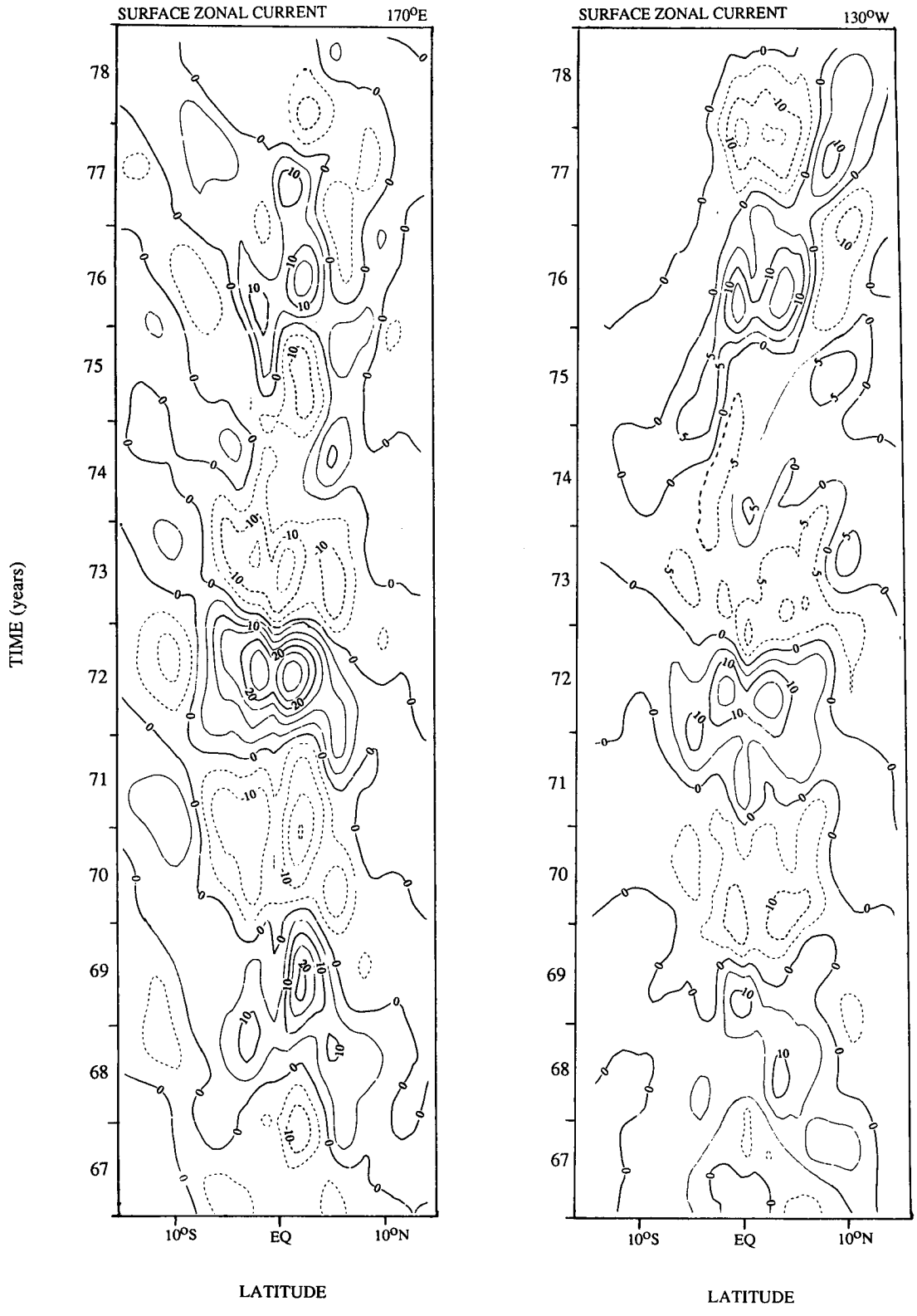

FIG. 10. The same as Fig. 9 but for surface zonal current (cm s^{-1}).

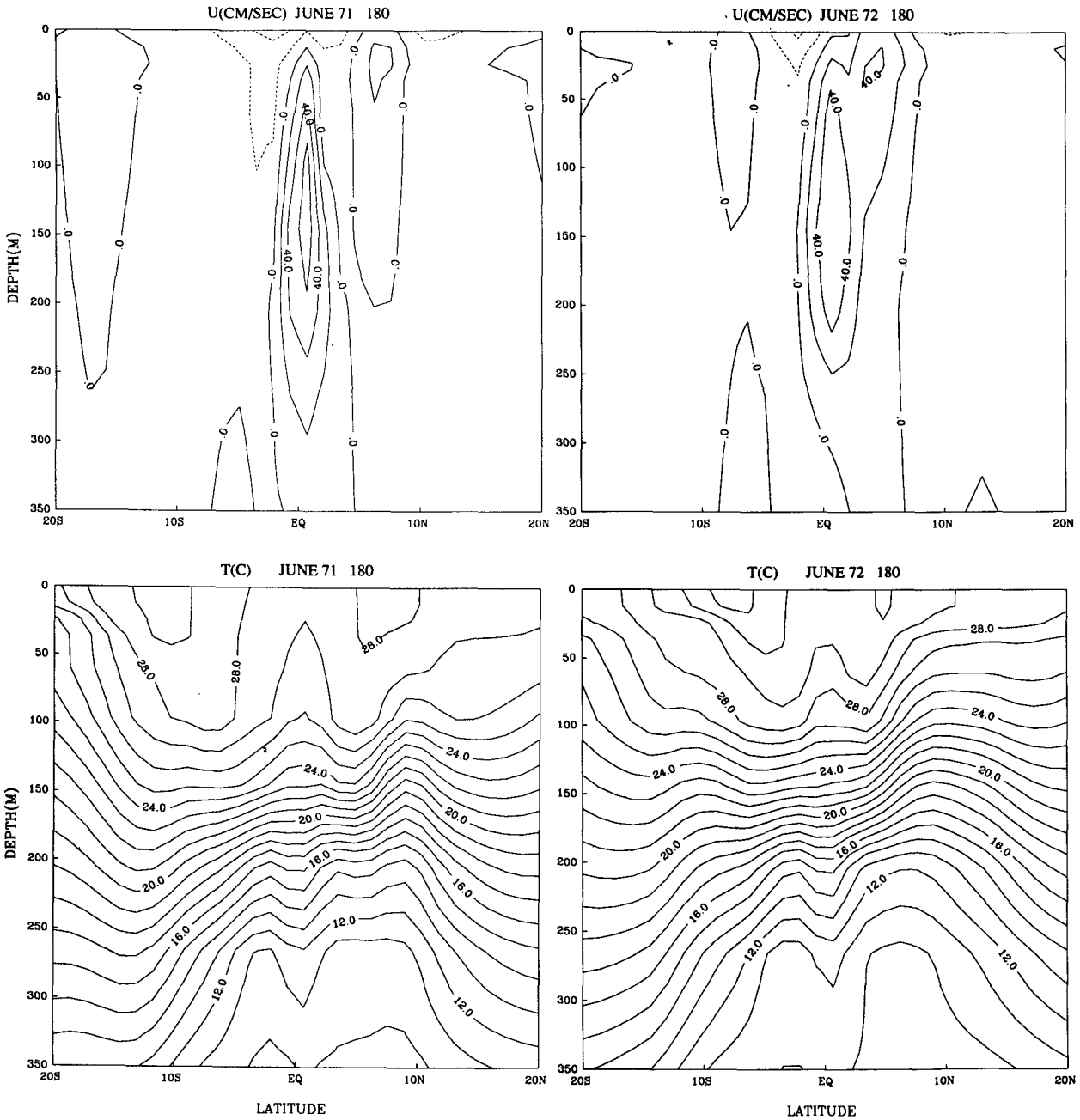

FIG. 11. Meridional sections of zonal current (cm s^{-1}) and temperature (°C) along 180° in June 1971 and 1972.

It combines spatial and temporal information to describe propagating features. Each eigenfunction is described by a sequence of maps, three in our case, which corresponds to conditions at three-month intervals. The first two sets, in Fig. 15, show that the evolution of the Southern Oscillation is in accord with the description of section 3. These two eigenfunctions account for 49.3% and 24.1% of the variance, respectively.

5. The heat budget

The discussion of section 3 emphasizes the zonal redistribution of warm surface waters during the Southern Oscillation: the thermocline is deep in the west and shallow in the east during El Niño, and the reverse is true during La Niña. There is, in addition, a meridional redistribution that becomes apparent when

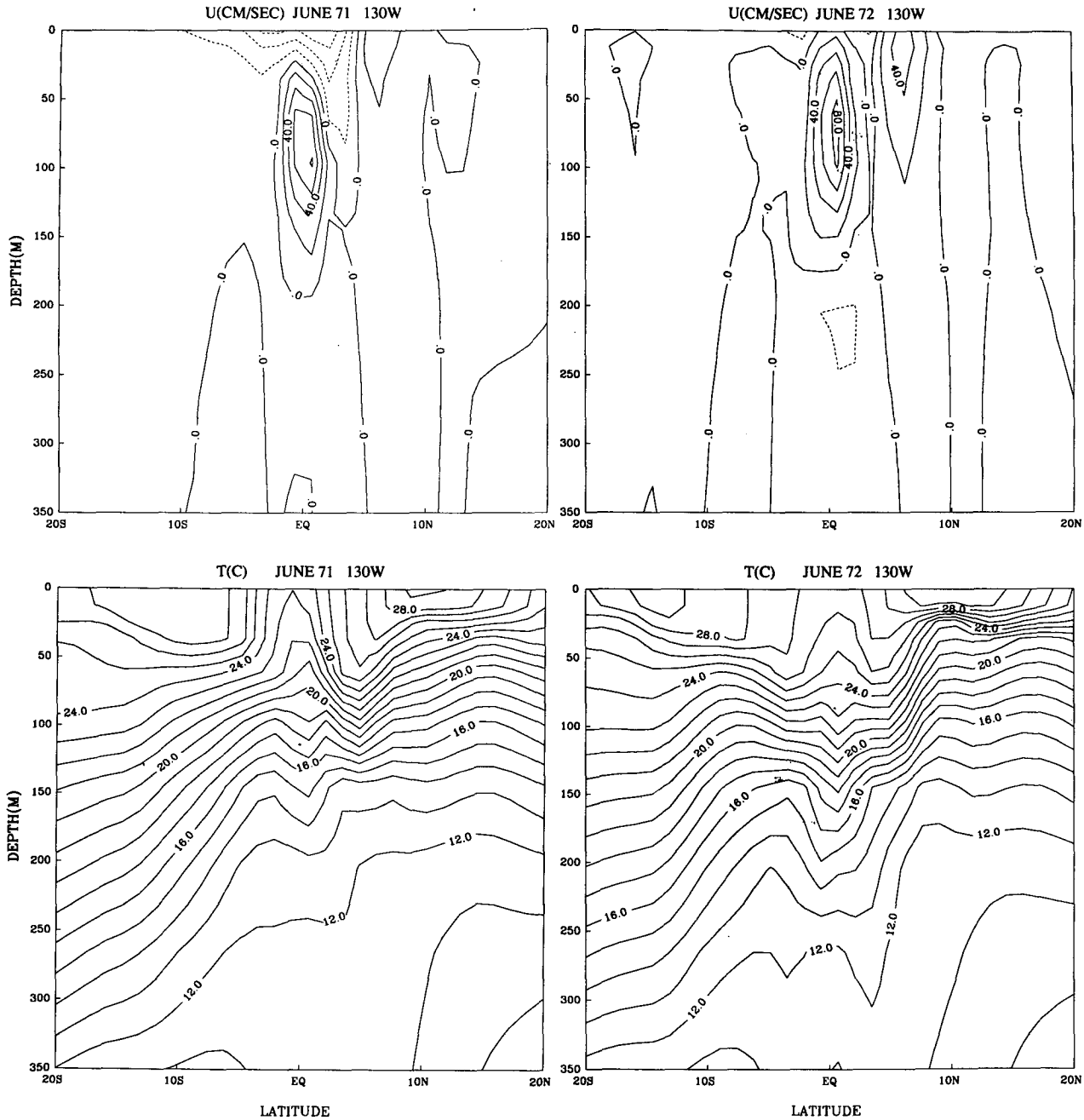

FIG. 12. The same as Fig. 11 but along 130°W.

the temperature is integrated vertically (from the ocean surface to the floor) and zonally (from the western to the eastern coast). Figure 16 shows how this heat storage varies as a function of latitude. Interannually, there is a large redistribution across approximately 6°N. The equatorial zone (6°N to 6°S) gains heat during the early stages of El Niño, up to May 1972 for example, and thereafter loses heat. The exchange is primarily with the region just north of 6°N. In the vertically and zonally integrated heat equation,

$$Q_t + (VT)_y = F,$$

the first term is the rate of change of heat storage, the second is the divergence of the meridional heat transport, and F is the flux across the ocean surface. In the

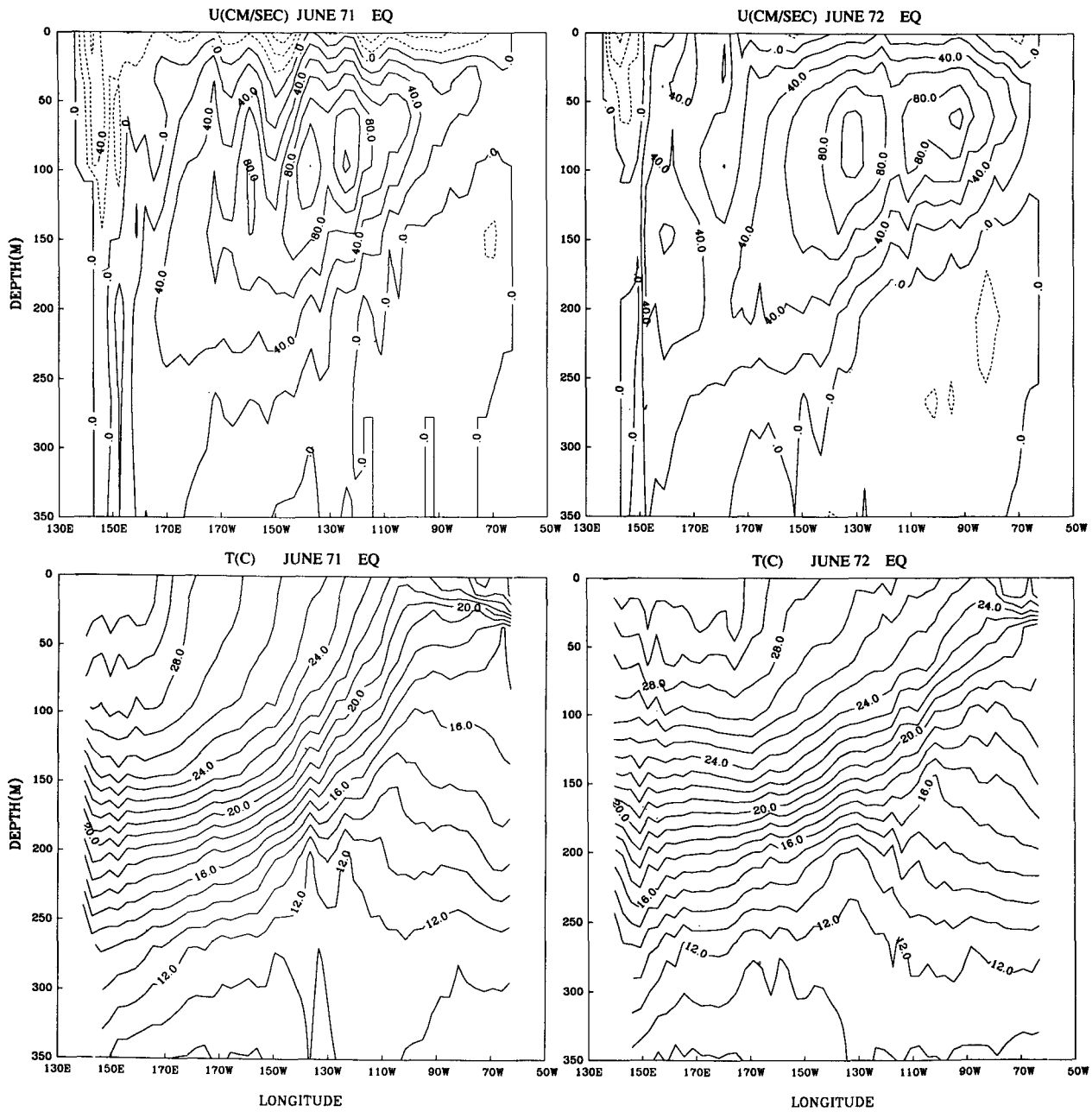

FIG. 13. Zonal sections of zonal current (cm s^{-1}) and temperature (°C) along the equator in June 1971 and 1972.

mean there is a flux of 1 petawatt of F across the surface of the equatorial zone of 6°S to 6°N that is transported poleward. The interannual fluctuation of F is only 10% as large and is negligible in comparison with the interannual variations of the other two terms. In other words, from an oceanic point of view, the Southern Oscillation is approximately an adiabatic phenomena. The extent to which this result is affected by the heat flux parameterization is unclear. Philander and Hurlin (1988), using a similar parameterization but simulating a different period—El Niño of 1982–83—found that increased evaporation because of high sea surface temperatures significantly affected the heat budget. A possible reason for their different result is the following. The areal extent and duration of warm sea surface temperature anomalies in 1982–83 exceeded those of the earlier El Niño episodes simulated here.

The striking aspect of Fig. 16 is that the changes of the meridional heat transport are large, not across the equator but near approximately 6°N. This is the mean

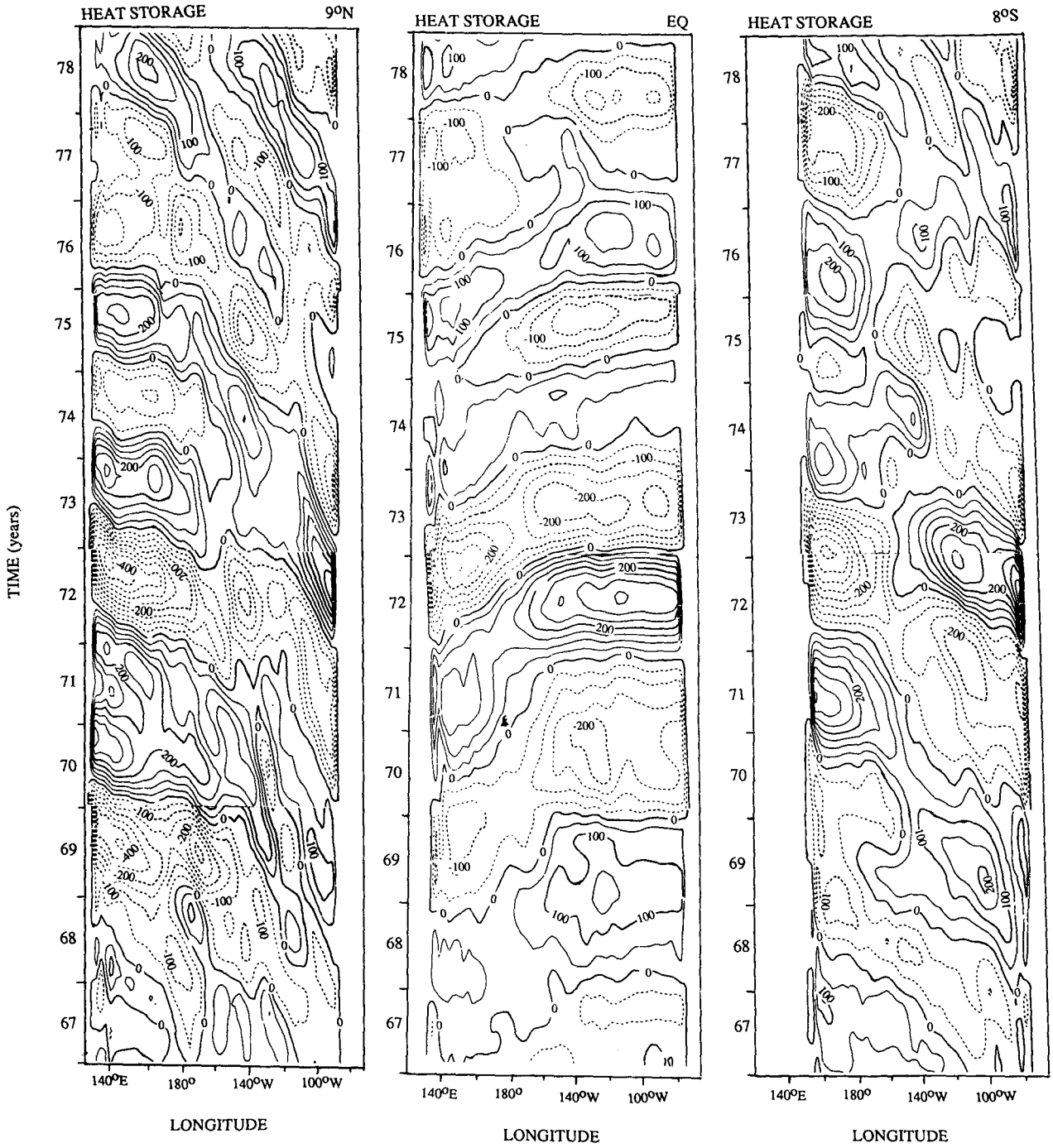

FIG. 14. Interannual variations in heat storage (°C m) at 9°N, along the equator and at 8°S.

position of the ITCZ. When the ITCZ is displaced equatorward during El Niño (see the January 1973 map of Fig. 6, for example), the northeasterly wind anomalies north of the equator cause a northward Ekman drift of warm surface waters so that the thermocline near the equator shoals while it deepens to the north of approximately 6°N. During La Niña the reverse happens.

6. Discussions

A realistic general circulation model of the ocean, forced with the winds observed over the tropical Pacific between 1967 and 1979, indicates that the interannual fluctuations between El Niño and La Niña have the structure shown schematically in Fig. 17. Westerly wind anomalies, in the form of an equatorial jet over the

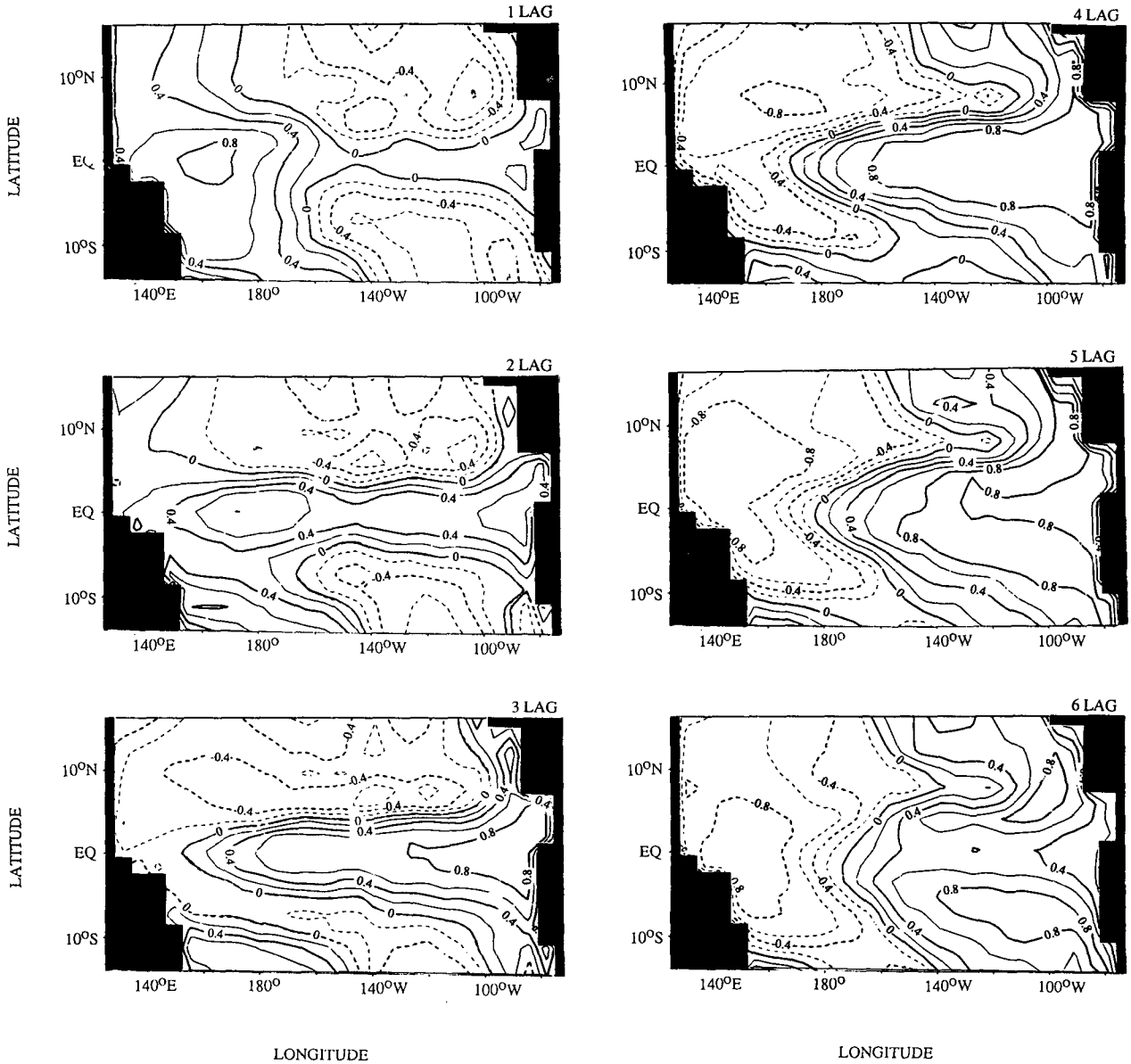

FIG. 15. Maps of the first and second extended EOFs. The six maps, at intervals of three months, show changes in patterns of heat storage during half a Southern Oscillation, an 18-month period.

western Pacific, induce thermocline displacements that are symmetrical about the equator with maxima off the equator in the west (because of the latitudinal shear of the wind there) but on the equator in the east. The temporal structure, shown in Fig. 14, is characterized by complex phase patterns because of the superposition of many waves plus wind-driven currents.

The picture of the Southern Oscillation that emerges from this study is a modification of the one originally proposed by Schopf and Suarez (1988), but the essence of their "delayed oscillator" mechanism remains: it is the "memory" of the ocean—that there is at any moment a delayed oceanic response to earlier winds—that permits a continual oscillation and gives the phenomenon predictability. In the delayed response Kelvin and Rossby waves are undoubtedly present but not explicitly, because many of them are superimposed and they cannot be isolated from the direct effect of the winds. The result is a complex phase pattern with speeds along the equator, not at the 150 cm s^{-1} of Kelvin waves but at a speed of 20 cm s^{-1} as in Fig. 14. The westerly wind anomalies over the western equatorial Pacific during El Niño depress the thermocline in the east and increase sea surface temperature there.

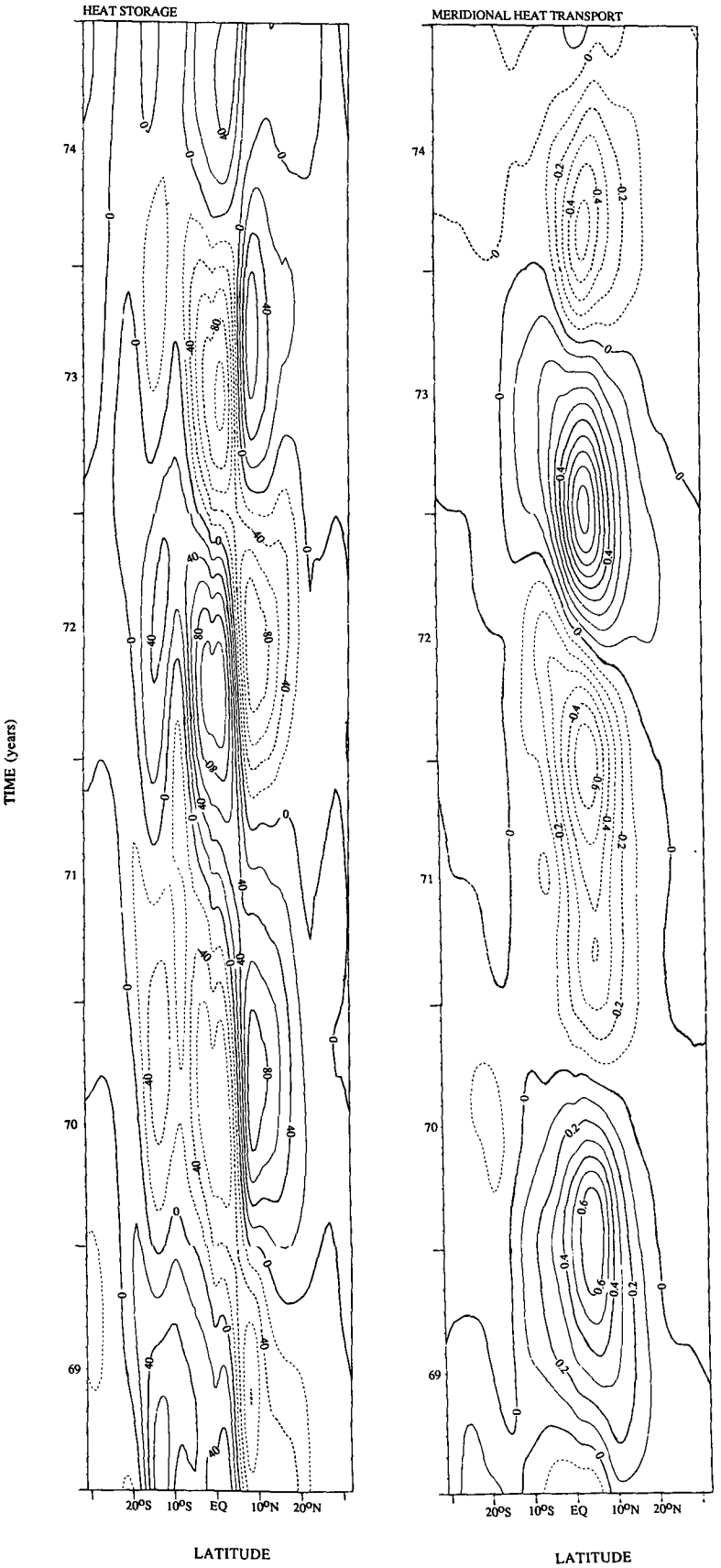

FIG. 16. Interannual variations of the zonally integrated heat storage (10^{12} J cm^{-1}) and meridional heat transport (10^{15} W). Solid (dashed) lines indicate deepening (shoaling) of the thermocline and poleward (equatorward) heat transport.

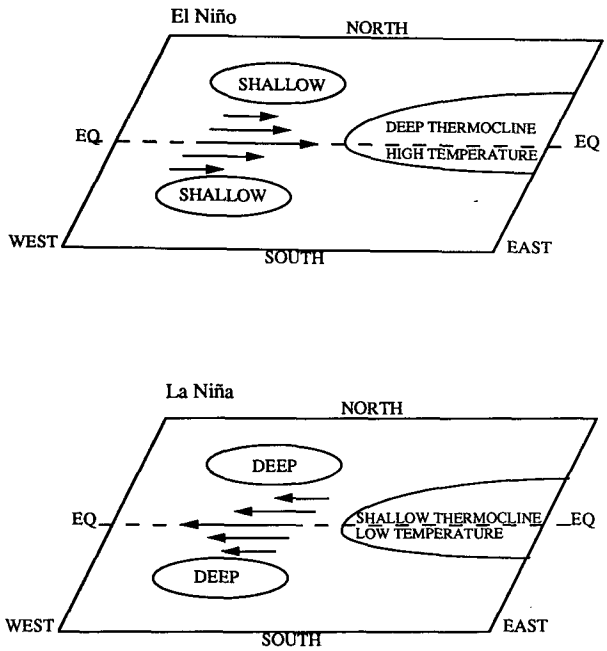

FIG. 17. A schematic diagram showing spatial distributions of surface wind stress, sea surface temperature, and heat storage at peak phases of El Niño and La Niña. The arrows indicate wind anomalies during El Niño. They depress the thermocline in the east where sea surface temperature anomalies are large. In the west they elevate the thermocline primarily off the equator, in the areas indicated by contours, because of their curl.

These winds also elevate the thermocline in the west, especially off the equator where the curl of the wind is large. In the absence of a western coast the off-equatorial elevations would disperse into Rossby waves and equatorial Kelvin waves. The latter reduce the deepening of the thermocline in the east. The presence of coasts in the west tend to channel the Rossby waves into equatorial Kelvin waves, further reducing the deepening of the thermocline in the east. The rate at which this happens and hence, the apparent phase speeds depend critically on the westerly wind anomalies and their latitudinal shear. At a certain stage the thermocline in the east stops deepening and eventually starts to rise. The associated change in sea surface temperature affects the winds in the west, El Niño decays, and in due course La Niña starts to develop.

The results summarized in Fig. 17 focus on those features that are common to all El Niño episodes in our simulation. Each El Niño, however, is distinct and has additional features that differ from one event to the next. In Fig. 3 [and in a version that covers a longer period (Chao 1990)] it is clear that sea surface temperatures along the equator sometimes exhibit westward phase propagation, an aspect emphasized by Rasmusson and Carpenter (1982), sometimes exhibit eastward phase propagation, in 1982 for example, and sometimes exhibit no zonal phase propagation. It is remarkable that the evolution of vertical thermocline movements is far more consistent from event to event than is the evolution of sea surface temperatures. The latter parameter clearly depends on far more than the thermocline depth; it also depends on advection and mixing processes, and their relative importance changes from one El Niño episode to the next. There is nonetheless an important aspect of the sea surface temperature changes that is common to all El Niño episodes: the confinement of large amplitudes to the eastern equatorial Pacific. This feature determines the salient aspect of the interannual wind fluctuations, namely, the equatorial jet over the western Pacific. Superimposed are wind variations that differ from one episode to the next. It is also possible for the evolution of El Niño to change from one episode to the next. For example El Niño started off the coast of Peru and grew in a westward direction in 1972, but in 1982 it first appeared in the west and grew in an eastward direction. The reason for such differences, which are absent from Fig. 17, are unexplained at this time.

Next, we turn to simulations of the Southern Oscillation. Several coupled ocean–atmosphere models reproduce aspects of this phenomena realistically, but the simulations differ from each other and from reality. The models of Meehl (1990) and Lau et al. (1992) reproduce interannual oscillations between states that resemble El Niño and La Niña, but the transition from one state to the other is characterized by pronounced westward phase propagation along the equator. Interactions between the ocean and atmosphere are important in these models, but the mode of interaction is not the "delayed oscillator" mode. It appears to be a type of mode recently investigated by Neelin (1991). The coupled general circulation models used by Philander et al. (1992) appear to capture the "delayed oscillator" mode. Their results, shown in Fig. 18, are in good agreement with those in Figs. 3 and 14 and in addition, have the change in latitudinal structure from west to east. The simpler coupled models of Zebiak and Cane (1987) and of Battisti and Hirst (1989) have much in common with the model of Philander et al. (1992). In Battisti and Hirst's results, shown in Fig. 19, the phase propagation along the equator clearly has spatial inhomogeneities with slow speeds in the central part of the basin where the wind fluctuations are most intense. If this region were displaced westward the results in Fig. 19 would closely resemble those in Fig. 18.

The results described here are from a realistic numerical ocean model forced with observed winds. Measurements are necessary to determine whether the results are accurate. The most useful measurements will be those that describe the structure of interannual variations in the depth of the thermocline in the western and eastern tropical Pacific. Particularly valuable will be data that permit plots such as those in Fig. 9 that

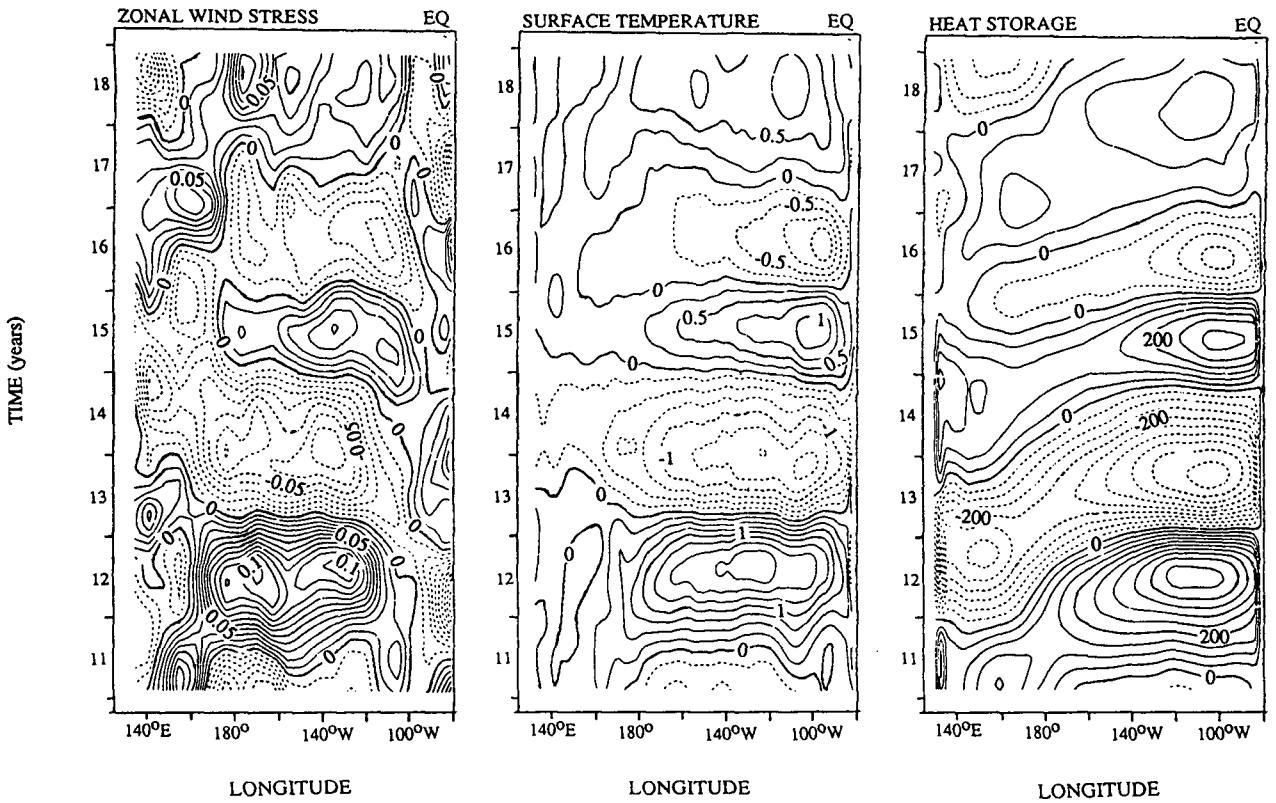

FIG. 18. Time–longitude plots along the equator of zonal wind stress (dyn cm^{-2}), sea surface temperature (°C), and heat storage (°C m) in the coupled ocean–atmosphere GCMs of Philander et al. (1992). Solid (dashed) lines indicate westerly (easterly) winds, warm (cold) waters, and deepening (shoaling) of the thermocline.

emphasize possible changes in latitudinal structure between the east and west, and those in Fig. 14 that depict changes in zonal phase propagation. The time series will have to be long enough to permit isolation of interannual fluctuations by means of low-pass filters, and will have to cover the western and eastern tropical Pacific. This is simply a statement that the Southern Oscillation is an interannual, basinwide phenomenon.

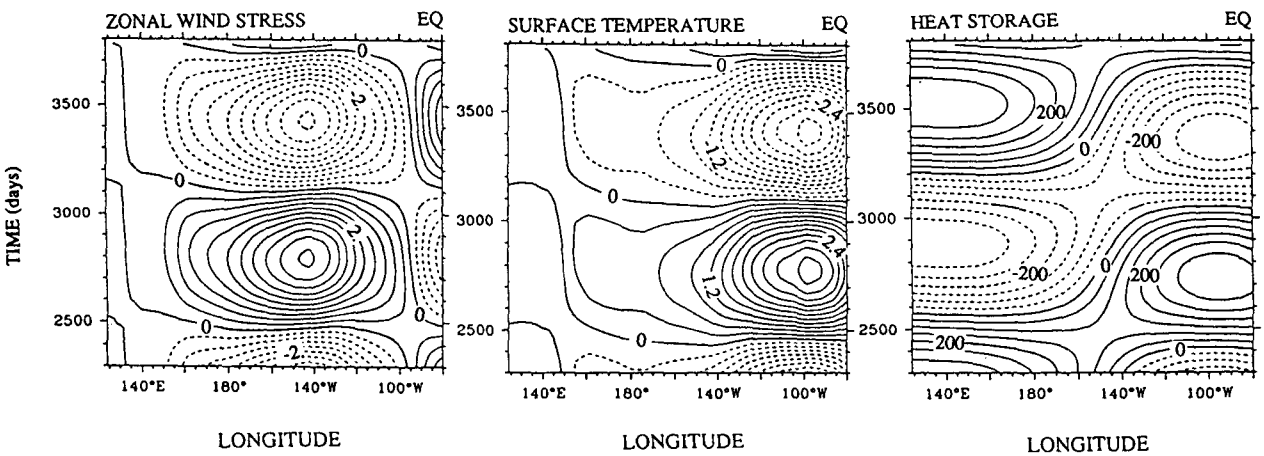

FIG. 19. Time–longitude plots along the equator of zonal wind stress (in nondimensional unit), sea surface temperature (°C), and thermocline depth (in unit of 5×10^{-2} m) in the coupled ocean–atmosphere model of Battisti and Hirst (1989). Solid (dashed) lines indicate westerly (easterly) winds, warm (cold) waters, and deepening (shoaling) of the thermocline.